Scholars Journal of Engineering and Technology

OPEN ACCESS

Abbreviated Key Title: Sch J Eng Tech
ISSN 2347-9523 (Print) | ISSN 2321-435X (Online)
Journal homepage: https://saspublishers.com

Analysis of Shock Formation in Fully Expanded Supersonic Flow in Convergent-Divergent Conical Nozzles Using Newly Derived Area-Mach Relation

R. C. Mehta[1]*

[1]Department of Aeronautical Engineering, Noolul Islam University, Kumaracoil 629180, India

DOI: https://doi.org/10.36347/sjet.2026.v14i07.003 | **Received:** 23.05.2026 | **Accepted:** 07.07.2026 | **Published:** 09.07.2026

***Corresponding author:** R. C. Mehta
Department of Aeronautical Engineering, Noolul Islam University, Kumaracoil 629180, India

Abstract | **Review Article**

Recently derived analytical area-Mach relation of quasi-one-dimensional isentropic flow for fully expanded supersonic flow inside a convergent-divergent conical nozzle is used to investigate shock formation and characteristics of numerically computed flow fields of the conical and the contour nozzles having identical area ratios and length. The flow fields inside the nozzles are numerically obtained by solving quasi-one-dimensional Euler equations and as well as axisymmetric turbulent compressible Navier-Stokes equations using finite volume method and explicitly integrated using multistage Runge-Kutta time marching method. Computed flow fields are analysed with the help of velocity vector and Mach contour to determine the influence of the geometry of the nozzle on flow behaviour. The variations of pressure and Mach number along the centre line and wall of the contour and conical nozzle are plotted to distinguish the flow characteristics. Formation of a hump in the centre line of pressure and Mach distributions due to shock formation of inside the conical nozzle is analysed using newly derived area-Mach relation. It can be extended to investigate the sonic boom of supersonic aircraft. The difference between CFD and quasi-one-dimensional isentropic results of centre line exit Mach number for conical and contour nozzle is found about -7.86% and 9%, respectively. Nomogram can be converted as a slide-rule for compressible gas dynamics.

Keywords: Area-Mach relation, Compressible flow, CFD, Convergent-divergent nozzle, Isentropic flow, Mach wave, Prandtl-Meyer function, Shock formation, Sonic boom.

1. INTRODUCTION

The fundamental gas dynamics equations for the well-known Laval nozzle [1] was invented in 1888 by Swedish inventor de Laval. Stodola's [2] area-Mach number relation is one of the most widely used expressions in compressible flow analysis. Majdalani *et al.,*[3] have derived a closed-form approximation for the inverted and more commonly used solution relating performance directly to the nozzle area ratio. Compressible flow through a convergent-divergent nozzle is customarily analysed using a quasi-one-dimensional isentropic flow equation described in a number of textbooks [4-12]. Comprehensive analysis of one-dimensional compressible fluid flow analysis is published by Daneshyar [13].

The method of characteristics [14, 15] in conjunction with the Prandtl-Meyer function and isentropic relation is employed to design a two-dimensional contour nozzle for obtaining uniform flow at the nozzle exit and minimum nozzle length. The method of characteristics is applicable to supersonic flow, and is widely applied to design contour nozzles because of its simplicity and the programming ease of the calculation procedure [6].

Shock formation inside a fully expanded supersonic convergent-divergent conical nozzle was first observed in 1963 by Darwell and Nadham [16] that compression waves could be generated in convergent-divergent nozzle geometries from the location where the curved throat section meets the diverging conical section, if the radius of curvature of the nozzle wall profile is discontinuous at that location. These compression waves can coalesce at the centre line at a point downstream to form a weak oblique shock. A series of technical papers published by Migdal and Landis [17] and Migdal and Kossen [18] showed that conical nozzles can have shock formation near the centre line due to intersection of Mach lines from flow overturning. The authors observed that

slight modifications to the curvature at the throat may reduce or eliminate shocks by accommodating the overturning of the flow.

Experiments conducted subsequently by Back *et al.,*[19, 20] and Cuffel *et al.,*[21] show this to be indeed true. The sharp drop in the Mach number along the centre line in Fig. 4 of [20] is due to the oblique shocks intersecting the centre line and the change in the shapes of the Mach number contours mentioned before is due to these incoming and reflecting weak oblique shock waves. These analyses predicted flow conditions near the nozzle axis which would lead to shock formation. This occurs where Mach lines originating just downstream of the circular arc-throat conical tangency meet the nozzle axis.

The computational fluid dynamics approach shows complete flow field features inside the nozzle by solving compressible Navier-Stokes equations. A numerical solution of the equations of motion for the nozzle has been computed using the finite-difference scheme to solve for the velocity and pressure has been presented by Riedelbauch *et al.,*[15]. The numerical simulations [16, 17] for a typical convergent-divergent conical nozzle show a formation of a hump in the centre line Mach number of the nozzle. It is found that the location and the shape of the hump on the centre line Mach number distribution are functions of the geometrical parameters of the nozzle such as semi-cone angle of the divergent section of the conical nozzle [15] and contour profile [22] of the bell nozzle. Method of characteristics predictions of supersonic flow through conical nozzles shows shock formation where characteristics originating just downstream of the tangency between the conical divergent section and throat curvature section approach the nozzle axis. This shock is not associated with overexpanded nozzle operation. Additionally, it was suggested that a conical divergent section could be attached after this point to achieve a shock-free flow with a simpler design than proposed by Rao [23] and Shmyglvesky [24].

An analysis analytical expression of area-Mach of a quasi-one-dimensional isentropic flow is employed in conjunction with the numerical solution of axisymmetric turbulent compressible Navier-Stokes equations with having identical the area ratio and the length of the conical and contour nozzles. A computed result shows a formation hump in the centre line of pressure and Mach number in the conical nozzle. The main aim of the present paper is to analyse hump in centre line pressure and Mach distribution with the newly developed analytical equation of area-Mach of a quasi-one-dimensional isentropic flow [25].

2. Derivation of analytical solution for Quasi-one-dimensional flow

2.1 Area-Velocity relation

We consider steady compressible adiabatic flow in a nozzle of varying cross-section as depicted in Fig. 1. Flow velocity is taken uniform over each cross-section of the nozzle. Employing the momentum equation and introducing the Mach number, this results relationship between density and velocity change. The relationship couples the area-velocity employing equations of continuity in a logarithmic differential form, Euler equation of motion with isentropic process [4] can be written as

$$\frac{du}{u} = \frac{1}{\left(M^2 - 1\right)} \frac{dA}{A} \tag{1}$$

The sign of $(M^2 - 1)$ is the determining factor in the qualitative nature of flow. Here we are considering the Prandtl-Meyer flow, that is, $M \geq 1$.

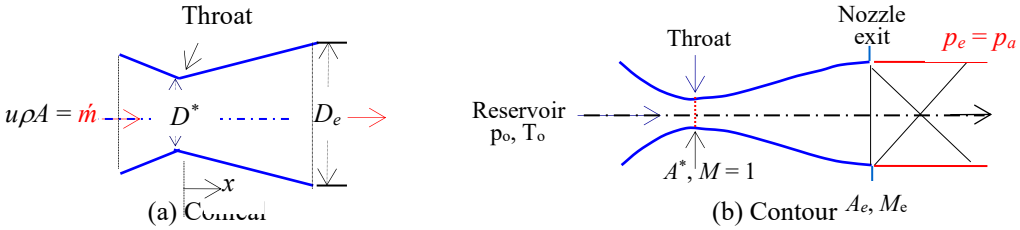

Fig. 1: Convergent-divergent nozzle

2.2 Prandtl-Meyer flow by turning

This section derives some quantitative relations between the infinitesimal flow through a Mach wave and a flow direction. The change in the flow parameters through a Mach wave will also be infinitesimal. The increment velocity *du* is in limit of algebraic increment in velocity *dV*. Now we considered a centred expansion wave at the throat. The simple expansion at a corner occurs through a centred wave, defined by a "fan" of straight line as delineated in Fig. 2(a). The flow up to the corner is uniform, at Mach M_1, and thus the leading Mach wave must be straight line, at the Mach angle ν_1. The terminating Mach line stands at the angle ν_2 to the downstream wall. We consider the limit of smooth flow, *i.e.*, the velocities and flow inclinations must be continuous but their derivatives may still be discontinuous on the Mach line.

Any deflection of the stream due to the presence body must begin at Mach wave. In Fig. 2(a), it changes its direction by the amount $d\theta$ at the point A corner point. $d\theta$ is positive in the clockwise direction for a deflection away from flow direction. The flow is the following wall, then the direction will also change at that point of corner, the turning will occur at the Mach line emanating from the corner point A. An expansion wave is isentropic throughout. The expansion at a corner occurs through a centred wave defined by a "fan" of straight Mach lines as shown in Fig. 2(b). From the geometry of Fig. 2(b), it is evident that $sin^{-1}(1/M) = \mu$, where μ the Mach angle, is half the angle of the Mach cone. A typical expansion over a continuous concave turn is shown in Fig. 2(c). The flow up to the corner is uniform, at Mach number M, and thus the leading Mach wave is ν_1. The terminating Mach line stands at the angle ν_2 to the downstream surface. The differential equation for an isentropic expansion by turning flow may be written as

$$\frac{1}{V}\frac{dV}{d\theta} = -\frac{1}{\sqrt{M^2-1}} \qquad (2)$$

where V is the resultant velocity and θ is the inclination of the velocity vector. It is important to mention here that the increment velocity du is in limit of algebraic increment in velocity dV. Equation (2) is scalar and relates change in speed to change in velocity direction. There is no pressure differential along the wave. Equation (2) is a scalar equation that relates the change in speed to a change in the velocity direction and also relates the infinitesimal change in velocity dV to the infinitesimal deflection $d\theta$ across the wave of vanishing strength. Flow properties are uniform along each Mach line. The magnitude of velocity at any point depends only on the flow direction at that point.

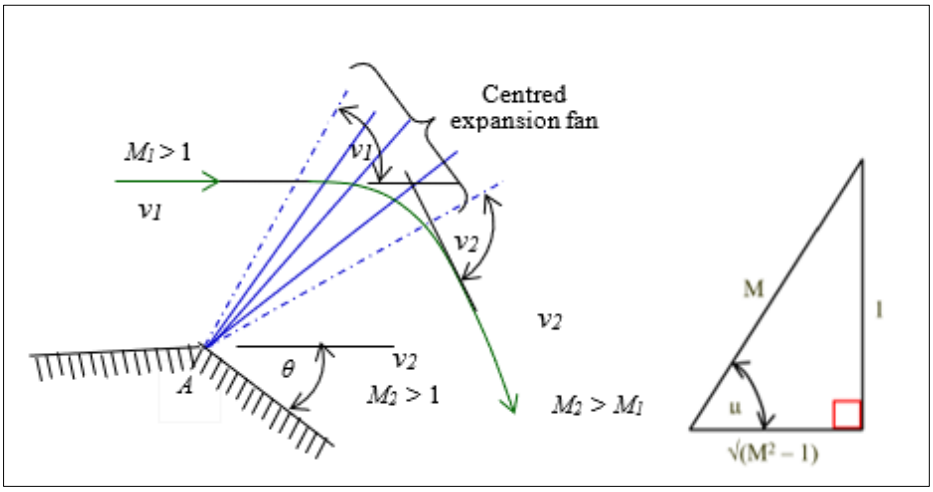

(a) Supersonic centred expansion wave over corner (b) Mach line

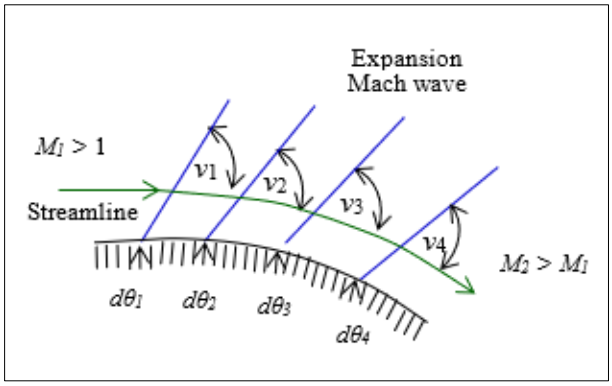

(c) expansion fan over a continuous, convex surface

Fig. 2: A typical expansion fan over a centred and a continuous, convex surface

2.3 Velocity-Mach relation

The differential equation for an isentropic expansion by isentropic turn across Mach wave may be written as

$$\frac{dV}{V} = \frac{1}{1+\frac{\gamma-1}{2}M^2}\frac{dM}{M} \qquad (3)$$

The exact solution of the above equation can be obtained by separating variables and described in the next section.

2.4 Analytical solution

The foundation of compressible flow through varying cross-sectional areas originates from the conservation of mass, momentum, and isentropic relation. The differential relationship connecting area variation *dA* to changes in the Mach number *dM* is expressed by substituting Eq. (2) in Eq. (3), we get

$$\frac{dA}{A}=\frac{\left(M^2-1\right)}{1+\frac{\gamma-1}{2}M^2}\frac{dM}{M} \tag{4}$$

To solve Eq. (4), we integrate both sides of the equation as

$$\int\frac{dA}{A}=\int\frac{1-M^2}{M\left(1+\frac{\gamma-1}{2}M^2\right)}dM \tag{5}$$

The analytical solution of the above equation can be evaluated by separation of variables and integrated to get

$$ln\,A=\frac{1}{2}\left(\frac{\gamma+1}{\gamma-1}\right)ln\left[2+(\gamma-1)M^2\right]-\frac{1}{2}ln\left[(\gamma-1)M^2\right]+C_1 \tag{6}$$

where C_1 is constant of integration. Equation (6) applies continuously through the isentropic turn; when integrated, it gives relation between Area and Mach number, which for the present we shall simply write in the form, where the area of cross-section of nozzle is function of Mach number and ratio of specific heats.

2.5 Analytical Integration and integration constant

The constant of integration of integration can be obtained using two stations of the nozzle. By cancelling out the constant C_1 between two separate cross-sections of a fully expended supersonic nozzle at A_1 and A_2 with corresponding M_1 and M_2 and yields as

$$ln\,A_1=\frac{1}{2}\left(\frac{\gamma+1}{\gamma-1}\right)ln\left[2+(\gamma-1)M_1^2\right]-\frac{1}{2}ln\left[(\gamma-1)M_1^2\right]+C_1 \tag{7a}$$

$$ln\,A_2=\frac{1}{2}\left(\frac{\gamma+1}{\gamma-1}\right)ln\left[2+(\gamma-1)M_2^2\right]-\frac{1}{2}ln\left[(\gamma-1)M_2^2\right]+C_1 \tag{7b}$$

Subtracting the above equations, we get

$$ln\frac{A_1}{A_2}=\frac{1}{2}\left(\frac{\gamma+1}{\gamma-1}\right)ln\left[\frac{2+(\gamma-1)M_1^2}{2+(\gamma-1)M_2^2}\right]-\frac{1}{2}ln\left[\frac{(\gamma-1)M_1^2}{(\gamma-1)M_2^2}\right] \tag{12}$$

Simplified and rewritten the above equation as

$$\frac{A_1}{A_2}=\frac{M_2}{M_1}\left(\frac{1+\frac{\gamma-1}{2}M_1^2}{1+\frac{\gamma-1}{2}M_2^2}\right)^{\frac{1}{2}\left(\frac{\gamma+1}{\gamma-1}\right)} \tag{13}$$

The derivation provides a rigorous mathematical bridge between indefinite spatial boundaries and local flow parameters. The equation evaluated between two boundaries or simplified directly into a ratio against the choked throat (*A/A**). Equation (13) is written at the nozzle throat conditions as:

$$\frac{A}{A^*}=\frac{1}{M}\left[\frac{2}{\gamma+1}\left(1+\frac{(\gamma-1)}{2}M^2\right)\right]^{\frac{1}{2}\left(\frac{\gamma+1}{\gamma-1}\right)} \tag{14}$$

The value of A/A^* is always greater than unity. The evaluation of indefinite integral is carried out by substituting $A_2 = A^*$, $M_2 = 1$ in Eq. (6). We can write as

$$ln\,A^*=\frac{1}{2}\left(\frac{\gamma+1}{\gamma-1}\right)ln(\gamma+1)-\frac{1}{2}ln(\gamma-1)+C_1 \tag{15a}$$

Simplified the above equations as

$$ln\,A^*=ln(\gamma+1)^{\frac{1}{2}\left(\frac{\gamma+1}{\gamma-1}\right)}-ln(\gamma-1)^{\frac{1}{2}}+C_1 \tag{15b}$$

The value of integration constant can be written as

$$C_1=ln\,A^*+ln(\gamma+1)^{\frac{1}{2}\left(\frac{\gamma+1}{\gamma-1}\right)}-ln(\gamma-1)^{\frac{1}{2}} \tag{15c}$$

$$C_1=ln\,A^*-ln\frac{(\gamma+1)^{\frac{1}{2}\left(\frac{\gamma+1}{\gamma-1}\right)}}{(\gamma-1)^{\frac{1}{2}}} \tag{15d}$$

$$C_1=ln\frac{A^*}{\left(\frac{(\gamma+1)^{\frac{(\gamma+1)}{2(\gamma-1)}}}{(\gamma-1)^{\frac{1}{2}}}\right)} \tag{15e}$$

The value of constant of integration for $\gamma = 1.4$ is as following

$$C_1=ln\left(\frac{A^*}{21.8576}\right) \tag{15f}$$

2.6 Pressure coefficient

For fully developed isentropic flow, the dynamic pressure is used for normalizing process and force coefficients, by isentropic flow, the pressure coefficient [3] may be written as:

$$C_p=\frac{2}{\gamma M_1^2}\left[\left(\frac{2+(\gamma-1)M_1^2}{2+(\gamma-1)M_2^2}\right)^{\frac{\gamma}{\gamma=1}}-1\right] \qquad M > 1 \tag{16}$$

The dynamic pressure depends on Mach number as well as the static pressure. Equation (13) can be simplified using Equation (16) as:

$$C_p = \frac{2}{\gamma M_1^2}\left[\left(\frac{A_1 M_1}{A_2 M_2}\right)^{\frac{\gamma}{(\gamma+1)}} - 1\right] \qquad (17)$$

3.0 Flow relations with respect to Mach number

The importance of Mach number and ratio of specific heats in determining the physical properties of steady, compressible, adiabatic or isentropic flow can be written

$$\frac{T_o}{T} = \left(1 + \frac{\gamma - 1}{2} M^2\right) \qquad (18)$$

If the flow is also reversible, the isentropic relation can be employed to express as T_o/T in terms of p_o/p or ρ_o/ρ. Thus, we get following isentropic relations

$$\frac{p_o}{p} = \left(1 + \frac{\gamma - 1}{2} M^2\right)^{\frac{\gamma}{\gamma - 1}} \qquad (19)$$

$$\frac{\rho_o}{\rho} = \left(1 + \frac{\gamma - 1}{2} M^2\right)^{\frac{1}{\gamma - 1}} \qquad (20)$$

The variables in these equations are Mach number and ratio of specific heats γ. Plots of Ratios of static to stagnation properties (T_o/T), (p_o/p), and (ρ_o/ρ) are shown in Figs. 3 and 4 for γ = 1.4. The relations between the thermodynamic variables are also tabulated in Tables 1 and 2 for γ = 1.4.

The variation of (A/A_e) versus Mach number is shown in Figs.3 and 4 having a very interesting behaviour for subsonic and supersonic Mach number. The (A/A_e) versus Mach number consists of subsonic and supersonic branches, so that (A/A_e) is double-valued except at $M = 1$, where $p^*/p = 0.528$ for $\gamma = 1.4$. If a throat of area A^* does not occur, the flow remains supersonic or subsonic throughout. Downstream of the throat of area A^*, the flow can either accelerate supersonically or decelerate subsonically, depending on the pressure ratio at the exit of the nozzle.

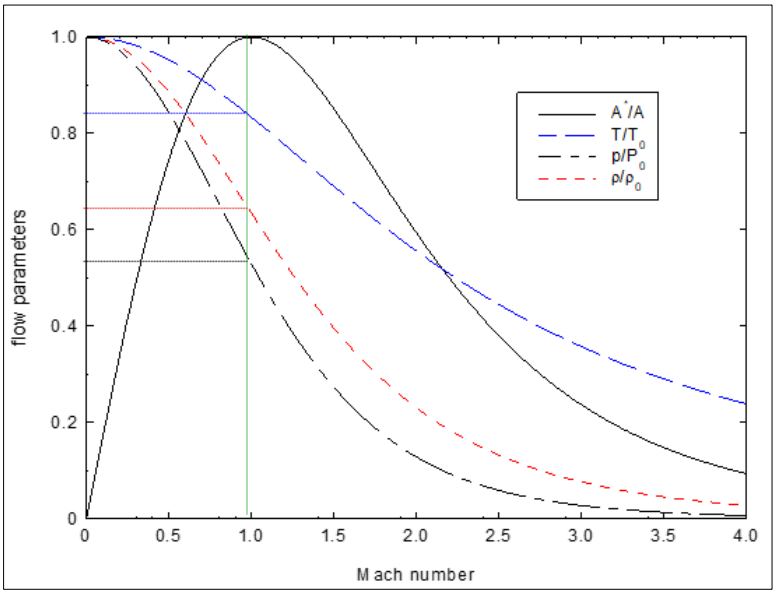

Fig. 3: Isentropic flow parameters versus Mach number

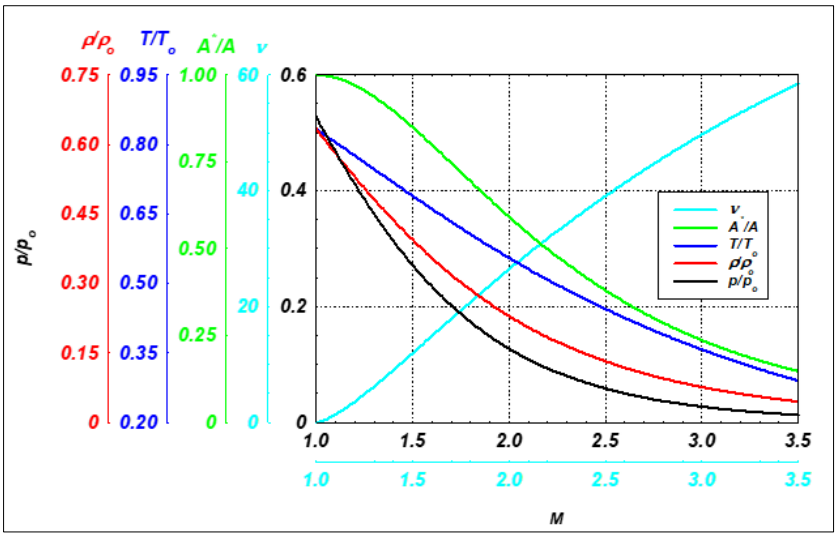

Fig. 4: Isentropic parameters for supersonic flow

Table 1: One-dimensional isentropic subsonic flow parameters

M	p/p_0	ρ/ρ_0	T/T_0	A/A^*
0.00	1.0000	1.0000	1.0000	0.0000
0.10	0.9930	0.9950	0.9980	0.1718
0.20	0.9725	0.9803	0.9921	0.3374
0.30	0.9395	0.9564	0.9823	0.4914
0.40	0.8956	0.9243	0.9690	0.6289
0.50	0.8430	0.8852	0.9524	0.7464
0.60	0.7840	0.8405	0.9328	0.8416
0.70	0.7209	0.7916	0.9107	0.9138
0.80	0.6560	0.7400	0.8865	0.9632
0.90	0.5913	0.6870	0.8606	0.9912
1.00	0.5283	0.6339	0.8333	1.0000

Table 2: One-dimensional isentropic supersonic flow parameters

M	p/p_0	ρ/ρ_0	T/T_0	A/A^*	ν (deg.)
1.00	0.5283	0.6339	0.8333	1.0000	0.0000
1.10	0.4684	0.5817	0.8052	0.9921	1.3362
1.20	0.4124	0.5311	0.7764	0.9705	3.5582
1.30	0.3609	0.4829	0.7474	0.9378	6.1703
1.40	0.3142	0.4374	0.7184	0.8969	8.9870
1.50	0.2724	0.3950	0.6897	0.8502	11.9052
1.60	0.2353	0.3557	0.6614	0.7999	14.8603
1.70	0.2026	0.3197	0.6337	0.7476	17.8099
1.80	0.1740	0.2868	0.6068	0.6949	20.7251
1.90	0.1492	0.2570	0.5807	0.6430	23.5861
2.00	0.1278	0.2300	0.5556	0.5926	26.3798
2.10	0.1094	0.2058	0.5313	0.5444	29.0971
2.20	0.0935	0.1841	0.5081	0.4988	31.7325
2.30	0.0800	0.1646	0.4859	0.4560	34.2828
2.40	0.0684	0.1472	0.4647	0.4161	36.7466
2.50	0.0585	0.1317	0.4444	0.3793	39.1236
2.60	0.0501	0.1179	0.4252	0.3453	41.4148
2.70	0.0429	0.1056	0.4068	0.3142	43.6216
2.80	0.0368	0.0946	0.3894	0.2857	45.7460
2.90	0.0317	0.0849	0.3729	0.2598	47.7904
3.00	0.0272	0.0762	0.3571	0.2362	49.7574
3.10	0.0234	0.0685	0.3422	0.2147	51.6498
3.20	0.0202	0.0617	0.3281	0.1953	53.4704
3.30	0.0175	0.0555	0.3147	0.1777	55.2221
3.40	0.0151	0.0501	0.3019	0.1617	56.9076
3.50	0.0131	0.0452	0.2899	0.1473	58.5299

3.1 Nomogram

The isentropic relations can be directly converted into a mechanical slide rule device to perform rapid computation of nozzle operating parameters, iteration free supersonic calculations. Because the Area-Mach analytical solution through logarithmic and power law scaling. These functions can be mapped onto sliding logarithmic scales. A nomogram for convergent-divergent is drawn using the above analytical relations. Figure 5 shows nomogram of Laval nozzle at ratio of specific heats equal to 1.4 for air. The present nomogram can be reconstructed with the help of a Python script.

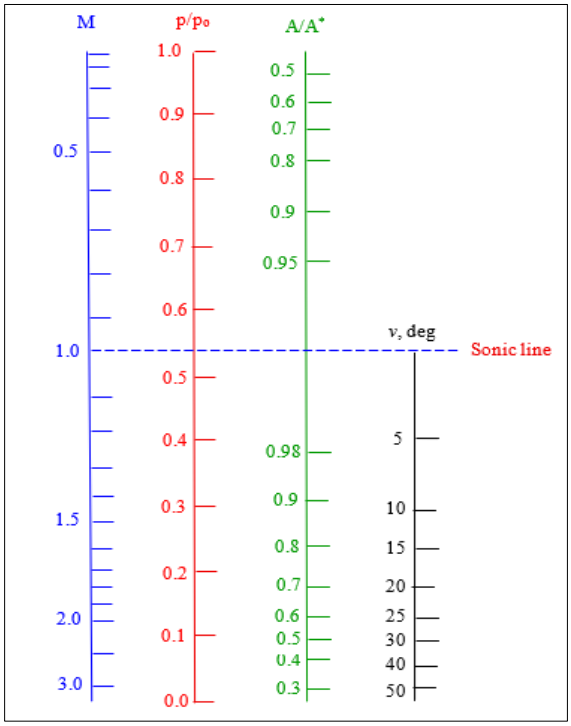

Fig. 5: Nomogram (slide-rule) for convergent-divergent

4.0 Compressible Fluid Dynamics Equations

4.1 Quasi-one-dimensional Euler Equations

A key element of the reduced-spatial domain model is to numerical solution of the pressure and Mach distributions inside the nozzle by solving the time-dependent, compressible quasi-one-dimensional Euler equations. The governing fluid dynamics equations can be written in conservation law form as follow:

$$\frac{\partial \boldsymbol{U}}{\partial t}+\frac{\partial \boldsymbol{F}}{\partial x}+\boldsymbol{S}=0 \qquad (21)$$

where

$$\boldsymbol{U}=A(x)\begin{bmatrix}\rho\\ \rho u\\ \rho e\end{bmatrix},\ \boldsymbol{F}=A(x)\begin{bmatrix}\rho u\\ \rho u^2+p\\ u(\rho e+p)\end{bmatrix},\ \boldsymbol{S}=\begin{bmatrix}0\\ p\dfrac{dA}{dx}\\ 0\end{bmatrix}$$

where A is the cross-sectional area of the quasi-one-dimensional equation for the nozzle. A is a continuous differential function that is independent of time. Therefore, A is a function of axial distance x and can be written as $A = A(x)$. Temperature is related to pressure and density by the perfect gas equation as

$$p=(\gamma-1)\rho\left(e-\frac{1}{2}u^2\right) \qquad (22)$$

where u is axial velocity of flow and e is internal energy.

4.2 Numerical solution

To facilitate to spatial discretization in the numerical method, the governing fluid dynamics Equations (1) is written in the integral form over a finite volume fixed in time as

$$\frac{d}{dt}\int_{\Omega}U d\Omega+\int_{\Gamma}F d\Gamma=\int_{\Omega}S d\Omega \qquad (23)$$

where Ω is the arbitrary control domain with the closed boundary Γ region. A contour integration around

the boundary of the cell is taken in the anticlockwise sense. The computational domain is divided into a number of small cell intervals in one dimension. The convective flux balance over the cell is approximated by taking average flux vectors on each grid cell with its magnitude and the outer normal for its direction. The scheme is a central difference scheme in the Cartesian grid. Spatial and temporal terms are decoupled using the method of line. We obtained a system of ordinary differential by applying Eq. (23) separating to each cell. These equations have the form as

$$\frac{d}{dt}\left(\Delta A_i U_i\right)+Q_i-D_i=0 \qquad (24)$$

where $\Delta\Omega_i$ is the cell volume and Q_i represents the net absolute flux out of the cell. The vector D_i is the local artificial dissipation term added in order to prevent odd even point decoupling and oscillations in the vicinity of large pressure gradients. The artificial dissipation term is described in the next section.

4.3 Artificial dissipation

The artificial dissipation model considered is based on the work of Jameson *et al.,*[26]. Local artificial damping is applied to ensure numerical dissipation needed for shocks is applied only locally and dynamically. The dissipation term is sum of second and fourth order dissipation terms, and can be expressed as

$$D(U)=\left(D_x^2+D_x^4\right)U_i$$

$$D_xU=\left(d_{i+1/2}-d_{i-1/2}\right)U$$

The dissipation fluxes are defined as blend of second and fourth-order in the conservative variables $\boldsymbol{U}$. The dissipative fluxes are written as

$$D_x^2U_i=\nabla x\left[\frac{A_{i-1/2}}{\Delta t}\left\{\varepsilon_{i-1/2}^2\left(\Delta_xU_i\right)\right\}\right]$$

$$D_x^4U_i=\nabla x\left[\frac{A_{i-1/2}}{\Delta t}\left\{\varepsilon_{i-1/2}^4\left(\Delta_xU_i^2\right)\right\}\right]$$

$$d_{i+1/2}=\frac{\Delta A_{i-1/2}}{\Delta t}\left[\varepsilon_{i-1/2}^{(2)}\left(U_{i+1}-U_i\right)-\varepsilon_{i-1/2}^{(4)}\left(U_{i+2}-3U_{i+1}+3U_i-U_{i-1}\right)\right]$$

where A is area of the cell and i is the location of the cell. The numerical value of constant ε influences the solution accuracy. The constant ε^2 and ε^4 are calculated using following relation

$$\varepsilon_{i-1/2}^2=\kappa^{(2)}max\left(\nu_{i-1},\nu_i\right)$$

$$\varepsilon_{i-1/2}^4=max\left[0,\left(\kappa^{(2)}-\varepsilon_{i-1/2}^2\right)\right]$$

Here ν is a shock sensing function based on pressure and can be written as

$$\nu_i=\left|\frac{p_{i+1}-2p_i+p_{i-1}}{p_{i+1}+2p_i+p_{i-1}}\right|$$

where $\kappa^{(2)}$ and $\kappa^{(4)}$ are 1 and 1/32. The blend of second and fourth difference provided third-order background dissipation in smooth regions of the flow and first-order dissipation in high gradient region.

4.4 Time-stepping method

The above spatial discretization reduces the governing equations to semi-discrete ordinary differential equations. Temporal integration is carried out using multistage Runge-Kutta time stepping method [26]. Suppressing the subscripts of operators is used to obtain the following steps:

$$U^{(0)} = U^n$$
$$U^{(1)} = U^n - \frac{2}{3}\Delta t\left(R^{(0)} - D^{(0)} \right)$$
$$U^{(2)} = U^n - \frac{2}{3}\Delta t\left(R^{(1)} - D^{(0)} \right) \quad (25)$$
$$U^{(3)} = U^n - \Delta t\left(R^{(2)} - D^{(1)} \right)$$
$$U^{n+1} = U^{(3)}$$

where artificial dissipation term evaluated only during first and second stages. The R is summation of the conserved variables over a control cell. The superscript n refers to an old time-step, n+1 the new time step. The stability condition for three stage time stepping is

$$\Delta t = \sigma \Delta t_{CFL}$$

where σ is a safety factor and Δt_{CFL} is

$$\Delta t_{CFL} = \left(\frac{u + c}{\Delta x} \right)^{-1}$$

where c is the speed of sound and Δx is the axial grid spacing.

4.5 Boundary conditions for quasi-one-dimensional Euler Equations

The following boundary conditions are used flow. At the subsonic inflow the stagnation pressure and temperature at the nozzle inlet are taken as 17x105 Pa and 3000o K, respectively. Supersonic exit conditions are imposed at the nozzle exit.

4.6 Two-dimensional/Axisymmetric Viscous Equations

The axisymmetric time-dependent compressible turbulent Reynolds-Averaged Navier-Stokes (RANS) equations considered in the present analysis are in strong conservation form and are solved using the FLUENT [27] software. The governing fluid dynamics equations can be written as

$$\frac{\partial \boldsymbol{U}}{\partial t} + \frac{\partial \boldsymbol{F}}{\partial x} + \frac{1}{r}\frac{\partial (r\boldsymbol{G})}{\partial r} + \frac{\boldsymbol{H}}{r} = 0 \quad (26)$$

where

$$\boldsymbol{U} = \begin{bmatrix} \rho \\ \rho u \\ \rho v \\ \rho E \end{bmatrix}, \boldsymbol{F} = \begin{bmatrix} \rho u \\ \rho u^2 + p - \sigma_{xx} \\ \rho uv - \tau_{rx} \\ (\rho E + p)u - u\sigma_{xx} - v\tau_{rx} + q_x \end{bmatrix}, \boldsymbol{G} = \begin{bmatrix} \rho v \\ \rho uv - \tau_{xr} \\ \rho v^2 + p - \sigma_{rr} \\ (\rho E + p)v - u\sigma_{xr} - v\sigma_{rr} + q_r \end{bmatrix}, \boldsymbol{H} = \begin{bmatrix} 0 \\ 0 \\ \sigma_+ \\ 0 \end{bmatrix}$$

Temperature is related to pressure and density by the perfect gas equation as

$$p = (\gamma - 1)\rho\left(e - \frac{1}{2}u^2 \right) \quad (27)$$

The coefficient of molecular viscosity is calculated according to Sutherland's law. The value of the turbulent Prandtl number Pr_t is assumed to take a constant value of 0.90. The Spalart-Allmaras model [28] has been employed to compute the eddy diffusivity using the transport equation for $\bar{\upsilon}$ as

$$\frac{\partial(\rho\bar{\upsilon})}{\partial t}+\frac{\partial(\rho\bar{\upsilon}u_i)}{\partial x_i}=G_\upsilon+\frac{1}{\sigma_{\bar{\upsilon}}}\left[\frac{\partial}{\partial x_i}\left\{(\mu+\rho\bar{\upsilon})\frac{\partial\bar{\upsilon}}{\partial x_i}\right\}+C_{b2}\left(\frac{\partial\bar{\upsilon}}{\partial x_i}\right)^2\right]-Y_{\bar{\upsilon}}+\bar{S}_{\bar{\upsilon}} \quad (28)$$

where $\bar{S}_{\bar{\upsilon}}$ is related to the scalar measure of deformation tensor and $f_{\upsilon 1}$ is the damping function. The turbulent viscosity μ_t is calculated using following relation

$$\mu_t=\rho\bar{\upsilon}f_{\upsilon 1}$$

where

$$f_{\upsilon 1}=\frac{\chi^3}{\chi^3C_{\upsilon 1}^3},\quad G_\upsilon=C_{b1}\rho\bar{S}\bar{\upsilon},\ \text{and}\quad Y_\upsilon=C_{w1}\rho f_w\left(\frac{\bar{\upsilon}}{d}\right)^2$$

The model constants for the Spalart-Allmaras [28] as $C_{b1} = 0.1355$, $Cb_2 = 0.622$, $Cw_2 = 3.206$, and $\sigma_\upsilon = 0.6667$. The above equations are solved using the FLUENT a commercial software [27]. The numerical simulation takes care of two-dimensional variation and viscous effects.

4.7 Boundary Conditions for Axisymmetric Viscous Equations

The following initial and boundary conditions are applied in the numerical analysis for fully expanded supersonic flow. At the nozzle wall, a no-slip condition is enforced together with adiabatic wall condition. At the subsonic inflow the stagnation pressure and stagnation temperature at the nozzle inlet are taken as 17×10^5 Pa and 3000^o K, respectively. The axial velocity is extrapolated. Supersonic exit conditions are imposed at the nozzle exit. The symmetric conditions are prescribed at the centre line of the nozzle. Wall functions are used at the nozzle boundaries to model the near-wall behaviour of the flow.

5.0 Conical and contour nozzle

When designing the nozzles for rocket engines we looked at the two basic types of nozzles, *i.e.* conical and contour nozzles. The conical nozzle is simply a cone shape described by the cone's half angle as viewed from the side as shown in Fig. 6(a). This type of conical nozzle contains no inflection as the propellants are expelled from the combustion chamber._Therefore, a conical nozzle is desired for solid rocket motor. One of the disadvantages of a conical nozzle is a significantly divergence loss at the exit.

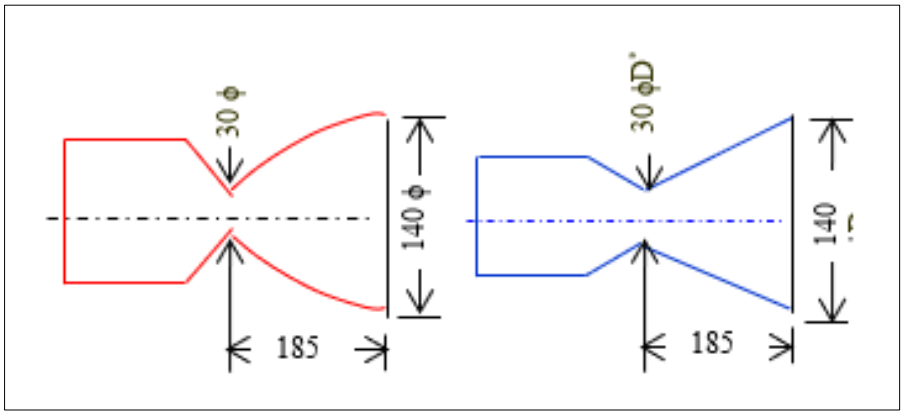

(a) Contour nozzle (b) Conical nozzle

Fig. 6: Geometrical details of (a) contour and (b) conical nozzles

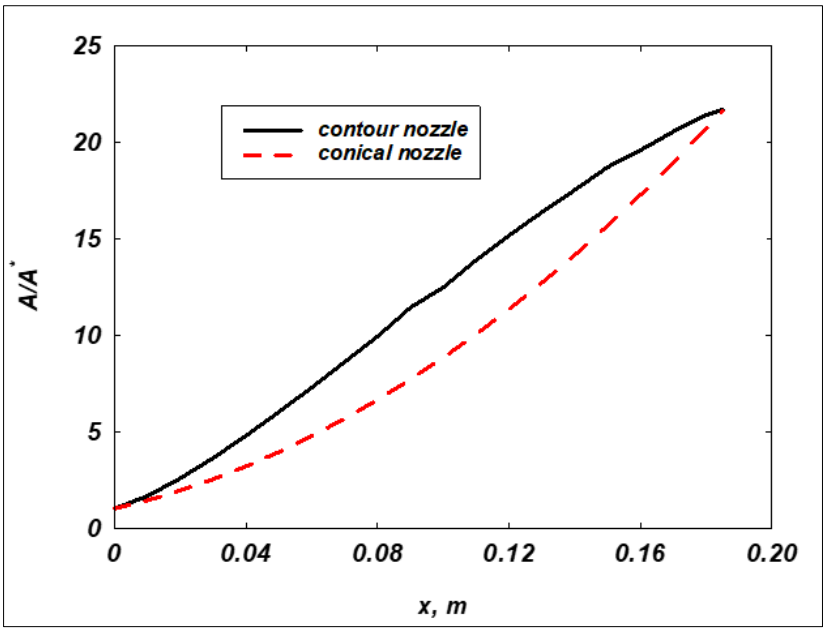

Fig. 7: Variation of Mach number in the conical and the contour nozzles

This inflection angle can be seen in Fig. 6(b) in respect to a contour or bell nozzle shape. This lack of inflection means that the nozzle is a straight line coming out of the throat to the exit. The advantages of a contour nozzle are that it reduces the divergence loss at the exit, it is less massive, and in turn more efficient than a conical nozzle. These characteristics make a contour nozzle much more efficient than a straight conical nozzle. For the sake of completeness the wind tunnel design had no length requirement but required only a uniform exit flow.

5.1 Nozzle Geometry and Grid Generation

The axisymmetric conical nozzle has is having convergent angle 30° and throat diameter $D^* = 0.03$ m. The semi-cone angle of the divergent section of the nozzle $\alpha = 16.557°$. The nozzle exit diameter is $D_e = 0.14$ m and is located at $L = 0.185$ m from the throat. The contour and the conical nozzles are having identical throat and the exit diameters as shown in Fig. 6 (a) and (b), respectively. Figure 6 displays the geometry of the contour and the conical nozzle. The variation of area ratio A/A^* with axial location is shown for the conical and the contour nozzles in Fig. 7. The maximum difference between the area ratios of the conical and the contour nozzles is seen at the axial location of about $x = 0.01$.

The computational grid is generated using the commercial package, GAMBIT [27]. The numerical simulations of the above-mentioned equations are carried out until the residues fall below 1.0×10^{-6} for all the flow variables. To investigate the sensitivity of the grid in the axial and the radial directions, a numerical investigation is performed for various grid sizes of 120 × 60, 160 × 60, 120 × 80, and 180 × 50. The grid independence check is presented in Ref. [25].

6.0 RESULTS AND DISCUSSION

6.1 Flow fields characteristics in conical and contour nozzles

The vector plot and Mach contour are shown in Fig. 8. It can be observed from the contour plots that there is no shock wave inside the nozzle. The flow is fully expanded. The Mach contours are not identical between two nozzles, though, they are having identical dimensions. These differences are attributed to contour and conical region of the nozzles.

A wall function approach [29] is used to bridge the viscous sublayer and the fully developed turbulent flow. The wall Mach number value is taken above the edge of the viscous sublayer and inside the fully turbulent region [29]. The centre line and wall variations of pressure and Mach number and in the first cell above the wall [29] of the conical and the contour nozzles are depicted in Figs. 9 to 12. The flow is shock free and fully expanded as can be observed from the centre line variations of pressure and Mach numbers in the nozzles. It is interesting to note that the formation of the hump in the conical nozzle is found between the axial locations of about 0.03 – 0.05 m as seen in Figs. 9 and 10. However, no hump formation is observed in the Mach profile of the contour nozzle. The distribution of the pressure and Mach number along the wall is influenced by the profile of the nozzle wall and the viscous effects. The average exit Mach number is higher in the contour nozzle as compared to the conical nozzle. The flow properties in the conical nozzle are analysed employing the relationship between the Mach number and the area ratio with quasi-one-dimensional isentropic relation.

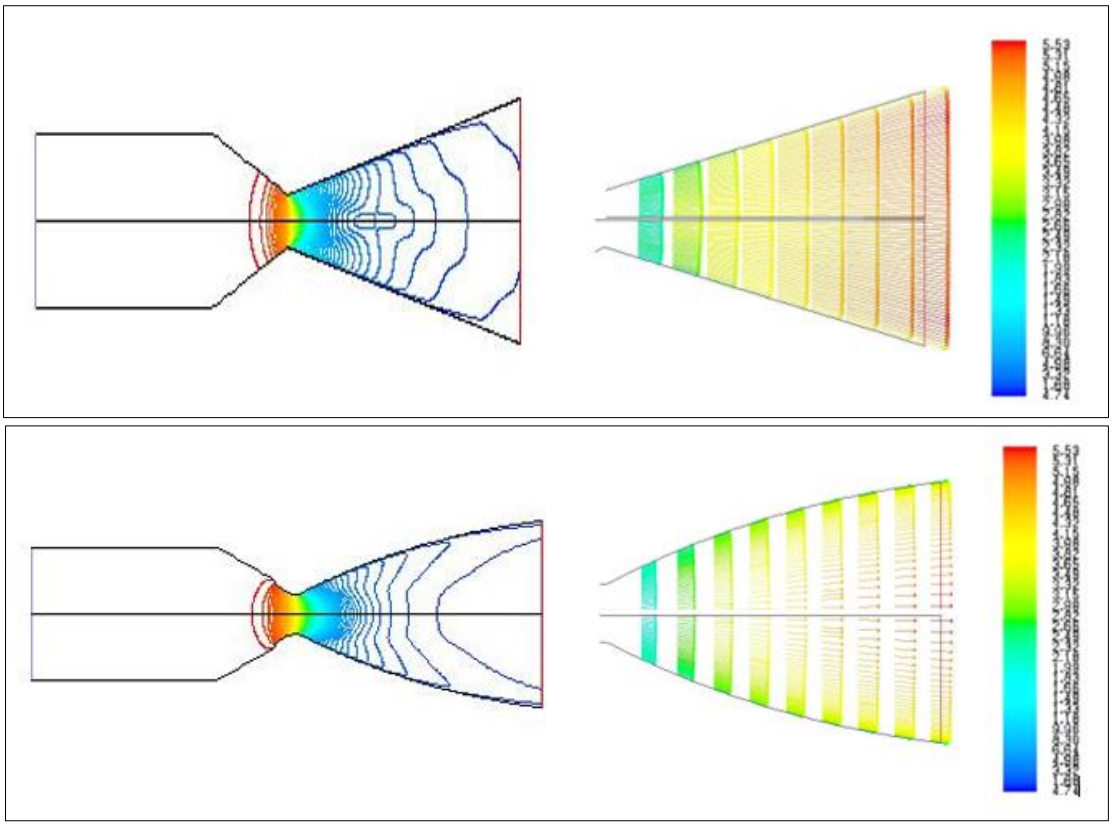

Fig. 8: Mach contours and vector plots in conical and contour nozzle

The maximum values of centre line Mach number for contour and conical nozzle are 5.21 and 4.39 respectively. The quasi-one-dimensional isentropic equation gives maximum value of centre line Mach number 4.83. The difference between computed values of centre line Mach number for conical and contour nozzle is having -7.86% and 9% as compared to the quasi-one-dimensional isentropic flow as tabulated in Table 3.

Table 3: Exit velocity in fully expanded conical and contour nozzles

Nozzle	A_e/A^*	Exit Mach number, M_e		
		CFD	Analytical	Error
Conical	21.623	4.394	4.83	9.10%
Contour	21.779	5.211	4.83	- 7.86%

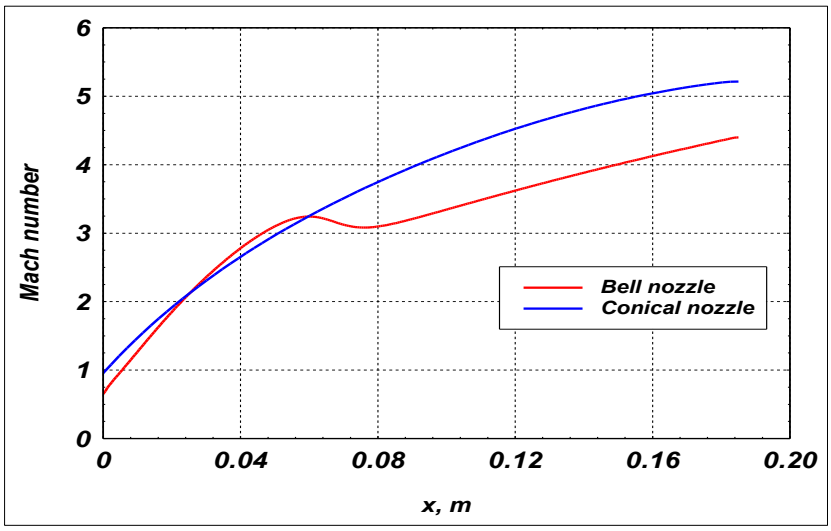

Fig. 9: Variation of centre line Mach number inside contour and conical nozzles

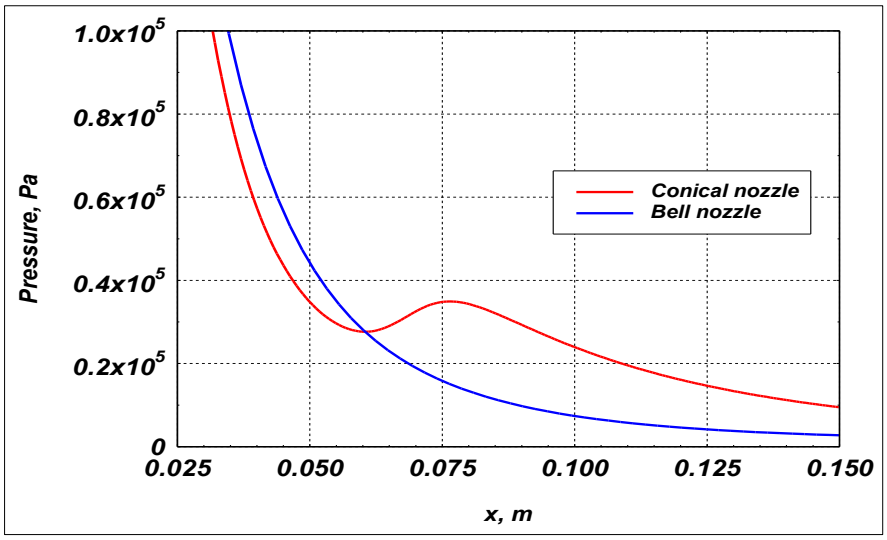

Fig. 10: Variation of centre line pressure inside contour and conical nozzles

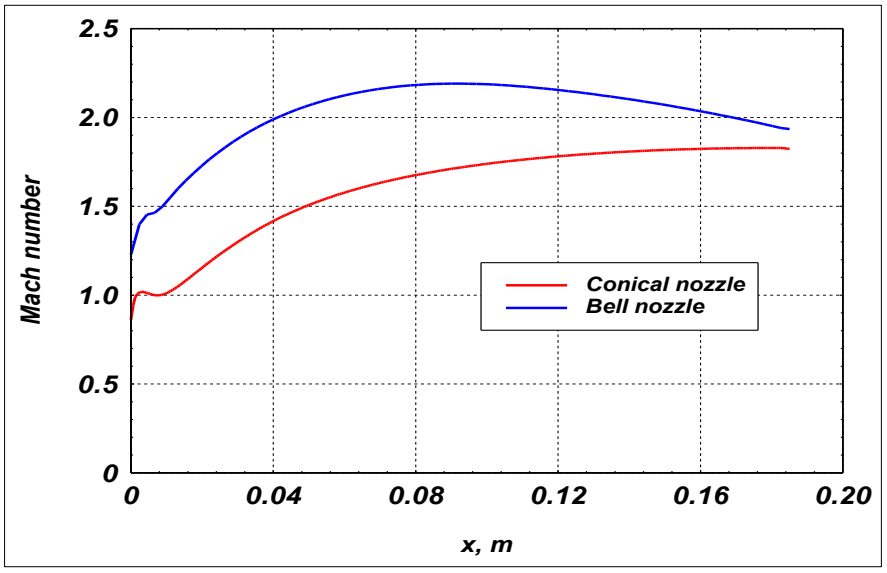

Fig. 11: Variation of wall Mach number inside contour and conical nozzles

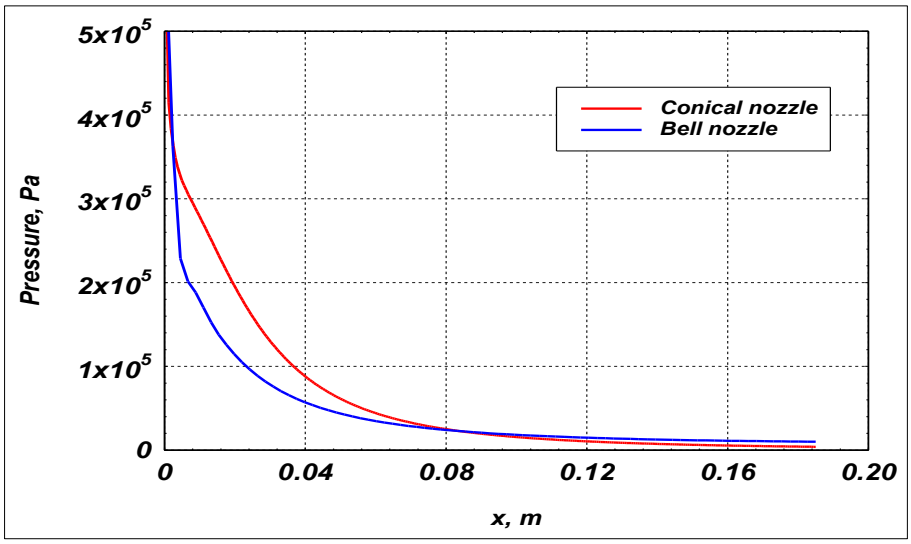

Fig. 12: Variation of wall pressure inside contour and conical nozzles

6.2 Formation of shock and hump inside conical nozzle

We can observe that the sectional Mach number is sensitive to the area ratio. The formation of the hump is actually a two-dimensional phenomenon which is observed in numerical simulations (both inviscid and viscous). The method of characteristics can be applied to compute the Mach number for the calculated value of the Prandtl-Meyer function.

The contour and the conical nozzles display different flow characteristics. The flow is shock free and fully expanded as can be observed from the centre line variations of Mach numbers in the nozzles. The distribution of the pressure and Mach number along the wall is influenced by the profile of the nozzle wall and the viscous effects. The average exit Mach number is higher in the bell nozzle as compared to the conical nozzle.

These contours appear very similar to those obtained using the method of characteristics [15] and [16] for inviscid flow in a similar geometry. They also agree very well qualitatively with the experimental results presented by Back *et al.,*[19] and Cuffel *et al.,*[21]. We have now analysed using the above derived Eq. (13). The shock wave strikes on the centre line and forms a hump in the Pressure and Mach distribution as depicted in Figs. 9 and 10, respectively. We have substituted the values of Mach number corresponding to the area of cross-section of conical nozzle. Thus coinciding the formation of the hump at those locations. It can be represented in a schematic sketch in Fig. 13. Pressure waves are generated due to corner shock generated from conical nozzles on the centre line. This observation is used to understand the sonic boom generated by supersonic aircraft in the next section.

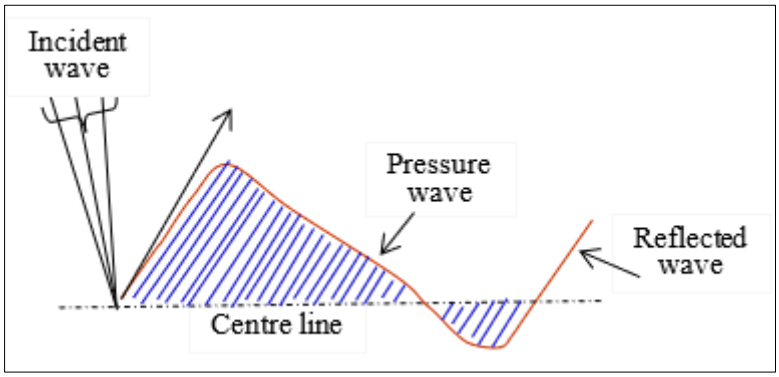

Fig. 13: Pressure wave generated by throat-cone of a supersonic convergent-divergent nozzle

6.3 Physical interpretation of Sonic boom of supersonic aircraft

The sonic boom is described by Saad [6]. The leading wave is the compression wave generated by the nose of the airplane trailing wave, which may create a continuous sonic boom, generated at the rear of the airplane as shown in Fig. 13. The numerical simulation of Park *et al.,*[30] indicates that the international state-of-the-art for near field computational fluid dynamics has a variation that is small enough for meaningful low-boom design and analysis for addressing the prohibition on overland supersonic aircraft. One of the remaining hurdles for practical supersonic flight is the reduction of sonic boom over-pressures on the ground to levels that would allow supersonic flight over land. Campbell *et al.,*[31]. The paper examines the use of two grid adaptation methods to improve the accuracy of the near-to-mid field pressure signature prediction of supersonic aircraft computed using the USM3D unstructured grid flow solver. A formulation has been presented by Rallabhandi [32] for the first time in literature that boom propagation and CFD are formally coupled for the purpose of obtaining gradients of a ground-based objective with respect to the aircraft shape design variables. A sonic boom ground signature sensitivity method has been developed using the discrete adjoint approach and augmented Burgers' equation.

7. CONCLUSIONS

Numerical solutions are obtained using steady compressible quasi-one-dimensional isentropic flow in fully expanded supersonic nozzles. The axisymmetric time-dependent compressible turbulent Reynolds-Averaged Navier-Stokes equations are solved to obtain flow field inside the fully expanded conical and contour nozzles. The difference between computed values of centre line Mach number for conical and contour nozzle is having -7.86% and 9% as compared to the quasi-one-dimensional isentropic flow.

A formation of a shock generated hump is observed in the centre line variations of Mach number and pressure of the conical nozzle and is found to be a function of the geometrical parameters of the nozzle. Very weak disturbances are propagating along the Mach lines in the throat region of the conical nozzle. The smooth flow over a centred expansion wave is considered to obtain a relationship between area-Mach. The analytical relation has been used to investigate the formation of hump, This flow phenomena may be extended to study sonic boom generated by supersonic

aircraft. Nomogram can easily be converted as a slide-rule for compressible gas dynamics using Python script.

Nomenclature

A = Area
a = speed of sound
D = diameter
L = length
e = total specific energy,
$\boldsymbol{F}, \boldsymbol{G}$ = flux vectors
$\boldsymbol{H}, \boldsymbol{S}$ = Source vector
M = Mach number (V/a)
p = static pressure
Pr = Prandtl number
q = heat flux components
t = time
u = axial velocity
$\boldsymbol{U}$ = conservative variables in vector form
V = resultant velocity
x, r = axial and radial coordinate
y = distance normal to wall
ρ = density
γ = ratio of specific heats
σ, τ = viscous stress
θ = deflection angle
υ = kinematic viscosity
μ = molecular viscosity
ν = Prandtl-Meyer function

Superscript
* = throat

Subscript
e = nozzle exit
o = stagnation
t = turbulent viscosity

REFERENCES

1. Anderson, J. D., Modern Compressible Flow: with historic prospective, Third Edition, McGraw-Hill Company, Singapore, 2004
2. Stodola, A., Steam and Gas Turbines: with a Supplement on the Prospects of the Thermal Prime Mover, McGraw-Hill Company, New York, 1927
3. Majdalani, J. and Maicke, B. A., Explicit Inversion of Stodola's Area-Mach Number Equation, Journal of Heat Transfer, **137**, July 2011, 071702-1-071702-7 DOI: 10.1115/1.4002596
4. Liepmann, H. W. and Roshko, A., *Elements of Gas Dynamics*, First South Asian Edition, Dover Publications, Inc., New Delhi, India, 2007.
5. Shapiro, A. H., *The Dynamics and Thermodynamics of Fluid Flow*, Vol. 1, Ronald Press, New York, 1953.
6. Saad, M. A., *Compressible Fluid Flow*, Prentice-Hall, Inc., Eaglewood Cliffs, New Jersey, 1985.
7. Imprie, B. W., Compressible Fluid Flow, Butterworth Heinemann Ltd, England, 1973
8. Oosthuizer, P. H., Compressible Fluid Flow, McGraw-Hill Education, New York, 1997
9. Kuethe, A. M. and Chow, C-Y, *Foundations of Aerodynamics,* 5th Edition, John Wiley & Sons, New Delhi, India, 2010
10. Anderson, J. D., *Foundations of Aerodynamics*, International Student Edition, McGraw-Hill Book Company, Singapore, 1985.
11. Bertin, J. J., *Aerodynamics for Engineers*, Pearson Education, Inc. New Delhi, India, 2006.
12. Rathakrishnan, E., *Gas Dynamics*, 6th Edition, PHI Learning Limited, New Delhi, India, 2017
13. Daneshyar, H., *One-Dimensional Compressible Flow*, Pergamon Press, Oxford, England, 1976.
14. Riedelbauch, S. and Welland, C., Inviscid Laval Nozzle Flow Field Calculation, *Journal of Spacecraft and Rockets*, Vol. 25, 1988, pp. 88-90.
15. Delussu, G. and Talice, M., Inviscid Supersonic Minimum Length Nozzle Design, Centre for Advanced Studies, CRS4, Research and Development in Sardinia, Italy, Dec. 17, 2002.
16. Darwell, H., and Badham, H., Shock Formation in Conical Nozzles, AIAA Journal,1(8), 1963, pp. 1932–1934. doi:10.2514/3.1965
17. Migdal, D., and Landis, F., Characteristics of Conical Supersonic Nozzles, ARS Journal, 32(12), 1962, pp. 1898–1901. doi:10.2514/8.6418
18. Migdal, D., and Kosson, R., Shock Predictions in Conical Nozzles, AIAA Journal, 3(8), 1965, pp. 1554–1556. doi:10.2514/3.3206
19. Back L. H., Massier P. F. and Gier H. L., Convective Heat Transfer in a Convergent-Divergent Nozzle, International Journal of Heat and Mass Transfer, 7, 1964, pp. 549–568. https://doi.org/10.1016/0017-9310(64)90052-3.
20. Back, L. H. and Cuffel, R. W., Detection of oblique shocks in a conical nozzle with a circular arc, AIAA Journal, 4(12), 1966, pp. 2219-2221. DOI: 10.2514/3.3881
21. Cuffel, R. F., Back, L. H. and Massier, P. F., Transonic Flowfield in a Supersonic Nozzle with Small Throat Radius of Curvature AIAA Journal, 7(7) pp. 1364-1366, 1969. DOI: 10.2514/3.5349
22. Mehta, R. C., Natarajan, G. and Bose, N. Fully expanded supersonic flow inside conical and contour nozzle, J. Spacecraft Rockets, 49(2), pp.422-425, 2012. doi.org/10.2514/1.A32195
23. Rao, G., "Exhaust Nozzle Contour for Optimum Thrust," Journal of Jet Propulsion, Vol. 28, No. 6, 1958, pp. 377–382. doi:10.2514/8.7324
24. Shmyglvesky, Yu. D., Some vibrational problems in gas dynamics of axially symmetric supersonic nozzle flows, Prilkadmaya Matematika I Mechanika, 21(2) 1957, 195-206.
25. Mehta, R. C., New Relationship Derived for Area-Mach, Area-Deflection and Area-Pressure for a Fully Expanded Convergent-Divergent Nozzle. Scholar Journal of Engineering and Technology, 14(5), 2026, pp. 247-254. doi.org/10.36347/sjet.2026.v14i05.006
26. Jameson, A., Schmidt, W. and Turkel, E., Numerical solution of Euler equations by finite volume method

using Runge-Kutta time stepping scheme, AIAA paper 81-1259, 1981.
27. Fluent 6.2, Computational Fluid Dynamics Software User Guide, Fluent Inc., Fluent India Pvt Ltd, 2010.
28. Spalart, P., and Allmaras, S., A One-Equation Turbulence Model for Aerodynamic Flows, AIAA paper 92-0439, 1992.
29. Saxena, S. K., and Mehta, R. C., Shock/Turbulent Boundary-Layer Interaction with Wall Function Boundary Conditions, AIAA Journal, 24(7), 1986, pp. 1207-1209.
30. Park, M. A. and Carter, M. B., Nearfield Summary and Analysis of the Third AIAA Sonic Boom Prediction Workshop C608 Low Boom Demonstrator, AIAA 2021-0345. doi.org/10.2514/6.2021-0345
31. Campbell, R., Carter, M., Deere, K. and Waithe, K., Efficient Unstructured Grid Adaptation Methods for Sonic Boom Prediction, AIAA 2008-7327. doi.org/10.2514/6.2008-7327
32. Rallabhandi, S. K., "Sonic Boom Adjoint Methodology and its Applications," AIAA Paper 2011–3497, 2011